Surface Science 723 (2022) 122101

Contents lists available at ScienceDirect

Surface Science

journal homepage: www.elsevier.com/locate/susc

Self-metalation of a free-base porphyrin on a metal oxide surface mediated by extended defects: Insight from ab initio molecular dynamics simulations

Osman Barış Malcıoğlu [a,b,c], Michel Bockstedte [*,a,b,d]

[a] Chemistry and Physics of Materials, University of Salzburg, Jakob-Haringer-Str. 2a, Salzburg A-5020, Austria
[b] Solid-State Theory, Friedrich-Alexander-Universitt Erlangen-Nrnberg, Staudtstr. 7B2, Erlangen D-91058, Germany
[c] Physics Department, Middle Eastern Technical University, Ankara, Turkey
[d] Institute for Theoretical Physics, Johannes Kepler University, Linz A-4040, Austria

ARTICLE INFO

Keywords:
Porphyrins
Metalation
Metal oxide
Magnesiumoxide
Low-coordinated sites
Ab initio Molecular Dynamics
Electronic structure

ABSTRACT

An important pathway for functionalization of porphyrin-based organic-inorganic structures is the metalation of porphyrins. Recently, the porphyrin metalation was demonstrated on different metal oxide surfaces, however, the underlying mechanisms regarding the role of the surface morphology, the substituted metal, and ligands are still under investigation. Here we address the adsorption and self-metalation of H2TPP on a MgO(001) surface with low-coordinated sites. We employ ab initio molecular dynamics simulations around room temperature to provide insight into dynamic steric effects. We observe that H2TPP is mobile on the pristine surface as the steric hindrance by phenyl rings prevents the physisorption of the macrocycle at a specific site. In contrast, step edges or kink sites provide anchor points exposing low-coordinated, reactive oxygen-sites to hydrogens of the macrocycle. We report a spontaneous proton transfer at these sites forming an intermediate complex before the metalation occurs. The energetics of the self-metalation reaction is modeled.

1. Introduction

Porphyrins form a versatile class of molecules [1] for a wide range of organic-inorganic hybrid materials [2–9]. Functionalization by substitution of ligands [10–13] enables a large variety of self-assembled porphyrin structures, including 2D and 3D architectures [14–17]. The ligation and the metalation of the porphyrin core [1,18,19] enable to tune properties on the molecular level for magnetic, catalytic, and sensing applications.

Metalation of free-base porphyrins at the surface has been achieved by the interaction with deposited metal adatoms [1,20]. Self-metalation was observed on specific metal surfaces like Cu, Ni, or Fe surfaces and involves intermediates, subsequent proton transfer, and release of H_2 [18,21,22]. Regarding metal oxides, the porphyrin-surface interaction was investigated at the surface, thin-films, or nanoparticles [11,20,23–33]. Self-metalation on metal oxides was recently demonstrated for instance for TiO_2 [23–26], different cobalt-oxides [30,31], or MgO [11,27–29], revealing a broad range of complex phenomena and mechanisms. These differ from the case of metal surfaces: (i) the stronger metal-oxygen bond affects the release of metal atoms and (ii) the formation of hydroxyl groups on the metal oxide is available. Consequently also low-coordinated adsorption sites and the morphology may play an important role.

For instance, at the TiO_2 (110) surface, besides self-metalation [25,26], metalation with Ni [20,23] and additional protonation of the porphyrin into the diacid form for a submonolayer coverage [24] was reported. Modeling based on density functional theory (DFT) shows that the porphyrin center is located on top of an oxygen bridge atom in these cases [26].

At MgO nanocubes and thick MgO films grown on Ag(001) [11,27,28] self-metalation was shown to occur at low-coordinated sites, such as corners of nanocubes, step edges, or kink sites but not at the surface terraces. Primarily, the reaction is driven by the energy gained from the formation of hydroxyl-groups in the exchange of the two protons for the metal atom released from the low-coordinated sites, as DFT calculations of the initial and final stage of the reaction with the porphyrins in the gas phase showed [11]. A distinct situation was recently found on thin MgO films on Ag(001) [29]. By tuning the work function of the MgO film on Ag(001), porphyrins got charged and underwent self-metalation to an extend that could not be explained by the abundance of residual low-coordinated sites. Despite the valuable insight provided by DFT-based modeling in this and the previous cases, several questions, in

* Corresponding author at: Institute for Theoretical Physics, Johannes Kepler University, Linz A-4040, Austria.
E-mail addresses: mbaris@metu.edu.tr (O.B. Malcıoğlu), Michel.Bockstedte@jku.at (M. Bockstedte).

https://doi.org/10.1016/j.susc.2022.122101
Received 1 November 2021; Received in revised form 18 April 2022; Accepted 19 April 2022
Available online 20 April 2022

particular regarding the reaction, remain open. These concern the adsorption at the low-coordinated sites, intermediate stages of the reaction pathway, and the related energetics. The present work provides insight into these questions regarding the self-metalation of the free-base porphyrin at the MgO (001) surface with a focus on low-coordinated sites by performing ab initio molecular dynamics simulation within the framework of density functional theory. Furthermore we shine light on the level alignment of the prophyrin and the metal-oxide substrate. In particular, we address different levels of ab initio theory including a semilocal functional, a hybrid functional and the GW approach. We demonstrate that the former, computationally feasible one for our molecular dynamics simulation provides a qualitatively correct description.

The article is organized as follows. In the subsequent theory section, we outline the theoretical approach and provide details of the calculation. The results are presented in the result section with three subsections. In the first one, we present the analysis of the molecular dynamics simulation, and the reaction energetics at the terrace, low-coordinated step edges, and kink sites. The simulations show the extend of steric effects in the dynamics and the occurrence of a spontaneous deprotonation reaction at the low-coordinated sites. The resulting scenario is shown in Fig. 1. The next section treats the electronic states of the adsorbed porphyrins in comparison with the molecules in the gas phase. This shines lights on the level alignment and hybridization of molecular and substrate states. We compare results obtained from density functional theory using the semilocal functional of the molecular dynamic simulations and a hybrid functional, as well as the GW approach. Finally, we report characteristic changes in the vibrational properties of the porphyrin by the adsorption and metalation at the terrace and step edges.

2. Theory

2.1. Overview over the general approach

The self-metalation of H2TPP to MgTPP on the MgO (001) surface is investigated in six calculation stages. First, the interaction of H2TPP with the pristine MgO (001) terrace, step edge, and kink site is simulated at 200 K. At the step edge and kink site, the porphyrin rapidly deprotonates and forms a HTPP-hydroxyl complex. The primary focus of this work is the reaction energies. The activation barriers depend heavily on the sample morphology at such low-coordinated sites [34], and has to be approached carefully taking into account the experimental conditions. This is beyond the scope of the present work; therefore, the metalation is simulated by directly exchanging the remaining Hydrogen with the Magnesium ion in the intermediate HTPP-hydroxyl complex. The MgTPP-hydrogenated defect complexes and MgTPP interacting with the pristine MgO (001) terrace are simulated in three separate calculations. The details of the calculation models are given below.

We perform ab initio canonical ensemble molecular dynamics (MD) calculations using the VASP simulation package [35] in order to access the binding energies. The electronic structure is described within DFT [36,37]. Standard density functionals fall short in accommodating long-range London dispersion interactions. A variety of different correction schemes have been developed that attempt to fix this shortcoming [38–40]. Among them, the DFT-D3 method [38] employed together with the PBE semilocal exchange-correlation energy functional [41] provides an overall good performance. The benchmark set includes similar organic molecules. Our results also confirm this for the crystalline phase of H2TPP [42]. In the following, we refer to this dispersion correction term as “VdW”. However, we also performed simulations using the local density approximation of the exchange-correlation functional (LDA) [43] yielding qualitatively similar results. Further aspects of the molecular dynamics simulations are given in the next subsection.

In order to investigate the alignment of porphyrin levels with the electronic states of the substrate and a possible hybridization with low-coordinated site, we analyse the Kohn–Sham states of the PBE-VdW calculations for selected configurations of the molecular dynamics simulations (cf. below) using the projected density of states of the molecule and the substrate. This analysis provides important insight. Nevertheless, the semilocal functionals are known for the short comings regarding, for instance, the underestimation of HOMO-LUMO gaps [44]. These short comings can be improved using hybrid functionals like the HSE06 functional [45] or by employing many-body perturbation theory within the GW approximation, which are however too demanding to be employed in molecular dynamics simulations. Therefore, we also investigate the correlation between the Kohn–Sham states and the

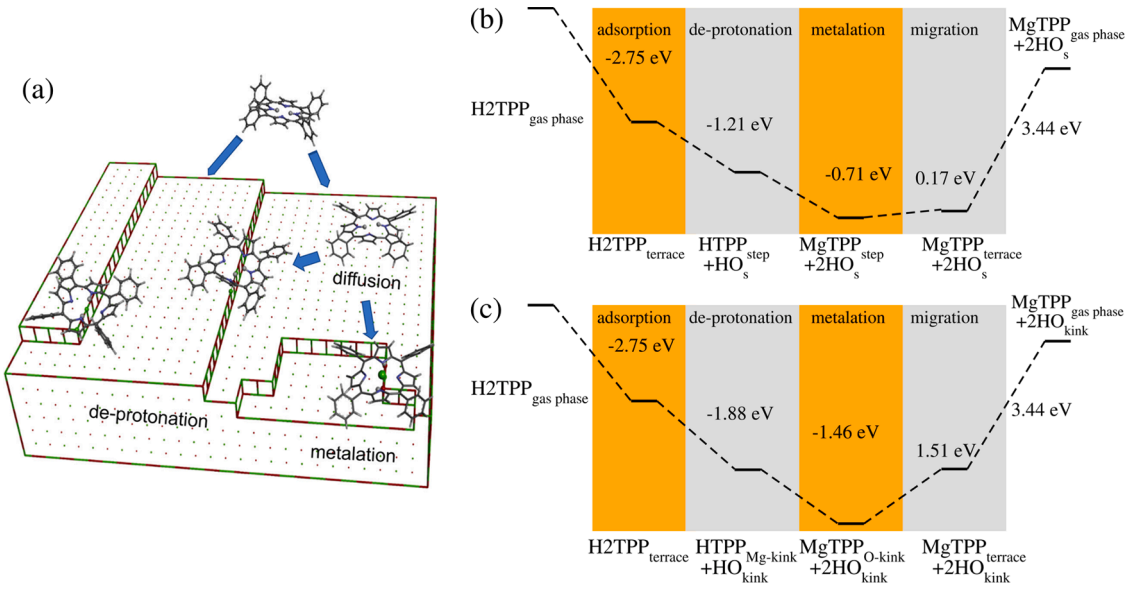

Fig. 1. Scenario of the metalation of H2TPP on the MgO surface via prototypical low-coordinated surface sites. (a) summarizes the six steps of the self-metalation pathway. First, H2TPP is physisorbed on the surface where it is mobile. Then the porphyrin migrates to step-edge or kink sites, deprotonates, and finally gets metalated. At this point, the energy cost of MgTPP migrating back to the surface and desorption from the surface is low. The reaction energies at each step in the self-metalation pathway are presented in (b) for step edge mediated metalation and in (c) for Mg-kink-mediated metalation.

Kohn–Sham/quasiparticle levels obtained with PBE-VdW, HSE06, and *GW* level of theory for selected configurations. In the latter approach we employ the standard G_0W_0 for the MgO surface and included self consistency for the prophyrin orbitals (GW_0). In both cases we use a DFT-LDA starting point, as this yields an excellent description of the ionization potential and electron affinity for both system [42]. Details of the *GW*-calculations are described in Ref. [42]. We observe that a simple scissor operator is sufficient to align the key porphyrine orbitals and MgO band edges with G_0W_0 calculated values. Thus the qualitative chemical arguments can be drawn from the molecular dynamics simulations. A detailed analysis on the relative level alignments can be found in the result section.

2.2. Molecular dynamics simulations

In the molecular dynamic simulations, the porphyrin and MgO substrate are represented in large supercells. The supercells allow for a large distance between periodic images of the molecules, adjacent steps, or kink sites, such that they can be considered isolated. The slabs are sufficiently thick to decouple the two surfaces or steps and kink sites in the respective cases. In the following, the details are given for each adsorption scenario.

The supercell used in the pristine terrace has dimensions ($a = 21.195$ Å, $b = 21.195$ Å, $c = 27.00$ Å, $\alpha = \beta = \gamma = 90^\circ$) and it contains a $Mg_{250}O_{250}$ slab ($5 \times 5 \times 2.5$ MgO conventional cell repetitions). The separation between in-plane periodic porphyrin images is initially 10 Å. The minimum distance observed throughout the simulation is 9.32 Å. The separation between the porphyrin and the lower end of the periodic slab image is a minimum of 11 Å. The step-edge supercell has dimensions ($a = 30.81$ Å, $b = 27.17$ Å, $c = 20.99$ Å, $\alpha = \beta = 90^\circ$, $\gamma = 118.11^\circ$), and the step edge itself is modeled by a $Mg_{350}O_{350}$ (5x5x2.5) slab that is shifted half a cell up at the middle. The initial in-plane separation of 10 Å between the porphyrin images is observed to be minimum 8.42 Å in the course of the MD run. The minimum distance between the porphyrin and the lower end of the periodic slab is 10 Å. The Mg kink supercell has dimensions ($a = 30.81$ Å, $b = 27.94$ Å, $c = 23.41$ Å, $\alpha = 92.36^\circ$, $\beta = 92.50^\circ$, $\gamma = 124.14^\circ$). The kink is modeled by $Mg_{358}O_{358}$ ($5 \times 5 \times 2.5$) slab. The minimal in-plane distance between the porphyrin and its images is 9 Å. The minimal distance between the porphyrin and the lower end of the periodic slab is 10 Å. The O-kink at the lower end was passivated by hydrogen.

Molecular dynamics simulations within the adiabatic or Born-Oppenheimer approximation was employed as implement in VASP [35]. At each timestep, the instantaneous Kohn–Sham electronic ground state is obtained using RMM-DIIS iterative scheme [46,47] with a total energy convergence criterion of 10^{-6} eV. Once the instantaneous electronic ground state is known, the forces are calculated from Hellmann-Feynman theorem [48]. The calculated forces are then used to integrate the Newtonian equations of motion for the ionic degrees of freedom via the Verlet algorithm [49].

The canonical ensemble with 200 K simulation temperature is realized using the Nosé thermostat [50,51]. In this thermostat, an additional degree of freedom is responsible for simulating the heath bath.

Its dynamics is controlled by a mass parameter Q and should equilibrate all vibrations of the system while remaining an external variable that does not directly interfere with the dynamics of interest. The MgO phonon spectrum [52–55] ranges approximately from 265 cm^{-1} to 800 cm^{-1} (corresponding to an oscillation period of 125 fs to 40 fs), whereas the infrared absorption spectrum (IR) of H2TPP and MgTPP [56,57] lie approximately between 500 cm^{-1} and 3400 cm^{-1} (corresponding to a oscillation period of 10 to 66 fs). We were able to replicate both H2TPP and MgTPP vibrational spectrum from the velocity autocorrelation function (VAF), using a mass parameter of $Q = 3 \times 10^{-29}$ a.u., a time step of 1.25 fs and a runtime of ~ 10.000 fs. For Q in this range, the characteristic period of the temperature fluctuations is approximately 68 fs. Our reference vibrational spectra have been obtained using NWCHEM [58]. We have employed the HSE06 range seperated functional together with a *maug-cc-pvdz* augmented correlation consistent polarized valence only double zeta basis set [59] for this purpose. The Hessian has been calculated using the forces obtained at the DFT-level relaxation. The infrared spectrum shown in Fig. 10 was calculated using perturbation theory and the HSE06 functional as implemented in NWCHEM [58]. Vibrational spectra of the adsorbed porphyrins at the terrace and low-coordinated sites were calculated from the molecular dynamics simulations using the VAF. Information on the vibrations of the whole porphyrin, its macrocyle and hydrogens was obtained by evaluating the VAF for the corresponding degrees of freedom only.

By analyzing the velocity distribution function (per degree of freedom) throughout the run time, we have seen no splitting into subsystems, and the result closely follows the Maxwell-Boltzmann distribution function as shown for selected examples in Fig. 2. Thus both the MgO and porphyrin form one common thermalized system with the employed parameters. Each molecular dynamics run contains at least 10 ps of equilibration time, followed by at least 10 ps used in statistical averages.

The calculation of adsorption, binding, and reaction energies involves substrates of different sizes. Therefore the calculations are based on the following energy differences

$$\overline{E}^{\text{MgO-site}}_{\text{xTPP}} = \overline{E}^{\text{MgO-site+xTPP}}_{\text{tot}} - \left\langle E^{\text{MgO-site}} \right\rangle \quad , \tag{1}$$

where $\overline{E}^{\text{MgO-site+xTPP}}$ is the time average energy of the porphyrin at the respective surface site as obtained form the molecular dynamics simulation and $\langle E^{\text{MgO-site}} \rangle$ denotes an ensemble average. The latter is calculated from the total energy of the corresponding fully relaxed geometry without the porphyrin and by adding the canonical averages for kinetic and potential energy in a harmonic approximation. For the geometry optimization a convergence criterion of 10^{-4} Å/eV on the residual forces was applied. As anharmonic effects should essentially arise from the dynamics of the porphyrin, we expect that this approximation has little effect on the results.

The metalation energy at the step edge (SE) $\overline{E}^{\text{SE}}_{\text{met}}$, involves the same substrate models and is calculated from

$$\overline{E}^{\text{SE}}_{\text{met}} = \overline{E}^{\text{MgO}_{\text{SE+defect}}+\text{MgTPP}}_{\text{tot}} - \overline{E}^{\text{MgO}_{\text{SE}}+\text{H2TPP}}_{tot} \tag{2}$$

The metalation at the kink defect was treated analogously. In all cases we took dipole-corrections into account where necessary.

3. Results and discussion

3.1. Diffusion and metalation of H2TPP

Our ab initio molecular dynamic simulations not only provides thermal averages of adsorption and reaction energies of the H2TPP regarding metalation, more importantly, it gives insight into the steric interaction of the four phenyl rings and the flexible macrocycle with the MgO surface terrace, the step edge, and a kink site. The overview of the different simulation scenarios and energetics at the step edge and kink site are given in Fig. 1a–c, respectively. Snapshots of the dynamics process are shown in Fig. 3. Videos of the respective simulations are provided as supplementary material. The simulation temperature is 200 K (see Section 2.2).

Our simulations at the MgO terrace show that H2TPP is mobile on the surface at the simulation temperature (see Fig. 3a). This seems counter-intuitive at first sight. Actually, H2TPP is a large molecule with several aromatic rings, and a VdW contribution of 2.58 eV to the adsorption energy at the terrace of 2.75 eV (see Fig. 1b), hence strong adherence to the surface can be expected. Using the LDA in our simulations, we obtain a similar absorption energy of 2.8 eV, although this

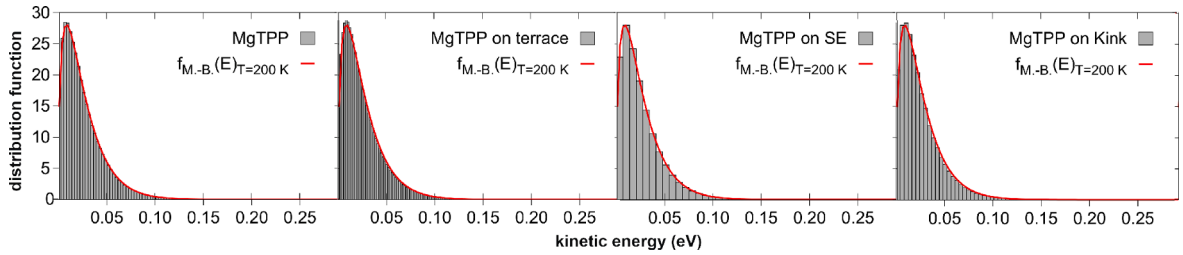

Fig. 2. Simulated velocity distribution function in comparison for MgTPP in the gas phase, at the terrace and step edge. The comparison with the Maxwell-Boltzman distribution verifies that all parts of our system are in equilibrium for the choice of the mass parameter Q.

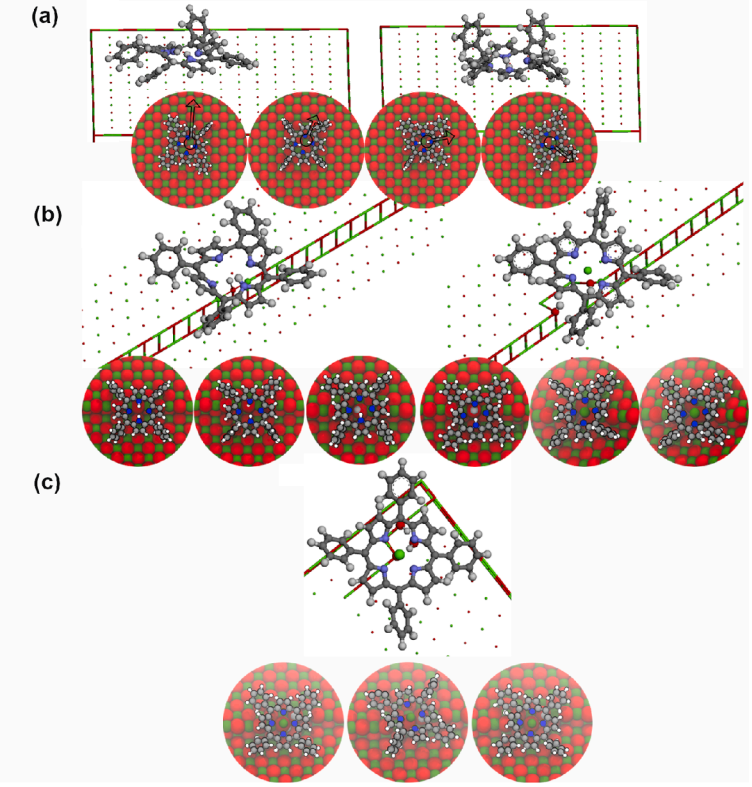

Fig. 3. Snapshots of specific dynamic processes from the simulation: (a) Mobility of H2TPP at MgO (001) defect-free terrace. Two extremes of the tug-of-war oscillation are shown in the top panels. If the molecule moves too far off, the phenyl rings orient to favor physisorption (left). When the macrocycle gets too close to the surface, the strained phenyl rings push the macrocycle back (right). This results in pedesis (bottom). (b) Deprotonation and metalation at the step edge defect. From left to right: H2TPP aligns itself on top of the step edge. The proton of the aminic nitrogen deprotonates to form O_{4c}-H. Iminic nitrogen starts interacting with Mg_{4c} near the O_{4c}-H. Metalation of HTPP to MgTPP is energy driven and requires transfer of another proton to form a second O_{4c}-H. (c) Metalation at an Mg-kink site creates an O_{3c}-kink.

approximation does not include a proper description of dispersion forces. Typically, the phenyl rings strongly prefer to orient out of the plane of the macrocycle. This has to be compared to an almost parallel orientation often found during the motion of the porphyrin (cf. Fig. 3a). In this way, the competition between the macrocycle-surface interaction and steric interaction between the phenyl rings and the macrocycle creates an oscillating tug-of-war. This, combined with the flexibility of H2TPP macrocycle and its rather complex vibronic landscape result in continuous stochastic propulsion. This aspect is clearly shown in the videos S1a and b in the supplementary material. While in the simulation shown in S1a the porphyrin moves about a Mg site, the video S1b shows the motion between different Mg sites. The latter simulation was performed using the LDA with different initial conditions. The PBE-VdW and LDA feature a quantitative similar description of the interaction in this case and hence we think that both simulations feature the properties of H2TPP at the terrace.

Now we turn to the reactive interaction of H2TPP with MgO steps. MgO planes with Miller indices higher than (001) facet into steps of (100) surfaces [60]. Such extended defects are typically observed on carefully prepared MgO(001) surfaces or thick MgO films on Ag(001). In our simulations (cf. Fig. 3b and video S2 in the supplementary material), we find that the porphyrin complexes with the extended step. The complex is by 1.21 eV (see Fig. 1b) is more stable than the physisorbed H2TPP at the terrace. When arriving close to the step edge, we observe that the porphyrin goes through a fast alignment process (<1 ps). In this process, an iminic nitrogen of the macrocycle positions on top of magnesium at the step edge. Then one of the aminic nitrogens in the macrocycle spontaneously transfers a proton to the nearest O_{4c} step edge atom. Almost instantaneously the deprotonated porphyrin, HTPP, forms an intermediate complex with the O_{4c}-H hydroxyl. In this complex the other iminic nitrogen now alignes and interacts with the hydroxyl while the deprotonated nitrogen aligns over the Mg step-edge neighbor of the O_{4c}-H group. During the subsequent simulation the residual aminic nitrogen shifts in a circular motion between the other Mg step-edge neighbor and the next O_{5C} neighbor, in part enabled by a favorable motion of the phenyl groups. In this motion the macrocyle is strongly twisted towards the surface due to the nitrogen-surface interaction. The observed spontaneous deprotonation, as well as, the strong N-Mg and N-hydroxyl interactions indicate that in the metalation reaction one of the Mg-neighbors of the O_{4c}-H group should be exchanged for the remaining hydrogen in a concerted motion involving also the phenyl rings. This eventually creates a hydroxylated Mg-vacancy at the step edge. Unfortunately, we could not observe the described metalation reaction directly in our straight forward molecular dynamics

simulations. The reaction rate of this process requires longer simulation times than we could afford in terms of computational costs with our approach. Given the importance of steric effects and the complex exchange mechanism, we expect a number of equivalent reaction pathways. Hence, neither a simple saddle point search will provide full insight into the complex mechanisms of the remaining exchange reaction.

Instead, we focus on the reaction energetics based on the outlined metalation. We transfer the remaining proton from the aminic nitrogen to form another O_{4c}-H group and lift the Mg slightly towards the macrocycle. Then an MgTPP – double hydrogenated defect complex is obtained straightforwardly by a relaxation step. We proceed with the MD calculations starting from this complex. In the subsequent simulations, the MgTPP re-aligns during MD simulation such that Mg is on top of one of the defect hydroxyl groups. The oxygen of this hydroxyl group is pulled towards the porphyrin, and it is slightly above the upper (001) terrace where the other hydroxyl group lies (see Fig. 3 and video S3 in the supplementary material). MgTPP – double hydrogenated defect complex formation is favored by 0.71 eV over the HTPP – single hydrogenated defect complex (cf. Fig. 1b).

Comparing these energetics with those of MgTPP physisorbed on the pristine MgO(001) terrace, and in the gas-phase, we predict that migration of this MgTPP back to a terrace will cost a relatively small energy of 0.16 eV (cf. Fig. 1b). The metalation at the step edge of H2TPP initially adsorbed on the terrace and transferred back to the terrace as MgTPP will yield an energy of 2.12 eV. In our simulation of MgTPP on the pristine MgO(001) terrace, we have seen that the metalated macrocycle adheres more strongly to the surface than H2TPP and the desorption of the molecule from the surface after having left the double hydrogenated step edge defect costs 3.44 eV (see Fig. 1b). Note that in our molecular dynamics simulations of H2TPP and MgTPP (see video S1a and S4 in the supplementary material), the two porphyrins move with the core, i.e. the center of two hydrogens or the Mg atom, about different surface atoms, namely Mg versus O. Due to the location of Mg at the center of the macrocyle and of the two hydrogens close to the aminic nitrogens, this leads in both cases to an enhanced interaction of the corresponding atoms with the surface O atoms while keeping a balance with the surface-interaction of the remaing atoms of the porphyrin. The observation of an overall better alignment of Mg with the surface O and of the four nitrogens with surface Mg during the motion indicates the origin of the larger adsorption energy of MgTPP.

Given the large desorption energy of MgTPP, we expect that a significant portion of the population of metalated porphyrins prefers to stay on the surface rather than to desorb, forming a film or self-assembled structures, dissipating the excess energy in thermal dissipation channels of the macrocycle. The overall reaction, converting gas-phase H2TPP to gas phase MgTPP is still energy driven by an energy gain of 1.45 eV (cf. Fig. 1b).

An important point we want to emphasize is that, when comparing the energetics we obtain from pure relaxation with the ensemble averages, there is almost an 0.3 eV difference in the reaction energy of the metalated porphyrin. For instance, after the metalation of H2TPP at the step edge to MgTPP, the binding energy to the reaction site obtained from ensemble average reads 0.16 eV, whereas this energy obtained from pure relaxation reads 0.7 eV. This is again a result from the dynamic tug-of-war effect of the phenyl rings: these prefer to be at an angle with the macrocycle, moving the reactive center away from the reaction site in competition with the attraction between the center and the defect.

In the simulation of H2TPP metalation at the Mg-kink, we follow similar steps as above. After de-protonation and during the subsequent metalation an O_{3c}-kink is formed (cf. Fig. 3c and the videos S5 and S6 in the supplementary material). The hydrogens from the macrocycle are captured by the adjacent O_{4c}, and O_{3c} such that the formed hydroxyl groups point their protons to fill the void left by the exchanged Mg atom (cf. Fig. 3, video S6 in the supplementary material). The HTPP-single hydrogenated kink defect is favored by 1.88 eV over the porphyrin at the surface and a further energy gain of 1.46 eV is yielded by the formation of the MgTPP-double hydrogenated kink complex (see Fig. 1c). These and the following energtics resulted from static calculations guided by the MD simulations, as it was difficult to converge the energy averages for the latter step with a reasonable effort. Finally, the dissociation from the kink site back to the terrace costs 1.51 eV, while subsequent desorption of MgTPP from the surface, leaving a double hydrogenated kink behind, will cost 3.44 eV (see Fig. 1c). The energy gain by the metalation at the Mg-kink exceeds the porphyrin binding energy to the hydroxylated kink site with respect to the terrace, so that MgTPP may leave the hydroxylated kink site. The overall reaction converting gas-phase H2TPP to gas-phase MgTPP is also energetically favorable by a smaller energy gain of 1.17 eV. As already noted by Schneider et al. [11] the energy gain in both metalation reactions stems from the exothermic exchange of Mg from the step-edge or kink sites for the two hydrogens from the porphyrin core. Here this energy gain is by $\sim$ 0.1 eV lower for the kink site.

3.2. Electronic states

Now, we turn to the alignment of molecular levels with the substrate and low-coordinated sites. For the analysis, snapshots are taken from the simulations. We calculate and compare the electronic structure obtained with the PBE-VdW functional with the results based on the HSE06 hybrid functional. We also illustrate the effect of many-body perturbation theory within the *GW* approach. The description of the porphyrin and MgO-substrate levels by *GW* or related approaches provides an excellent agreement with experiments such as photoemission, e.g. [42,44,61]. The discussion shines light on the electronic structure of the complex adsorbate systems and demonstrates that a qualitatively correct level alignment is achieved despite the known shortcomings of the PBE-VdW, thus validating its utilization in the MD simulations.

In order to see how the levels are typically aligned throughout the MD simulation, we have chosen snapshots well after equilibration, and relaxed the geometry with the same PBE-VdW functional to obtain an appropriate equilibrium point for our analysis. The partial density of states due to MgTPP and H2TPP along with a schematic representation of the position of surface and bulk states of MgO are presented in Figs. 4–6.

Various photo-physical properties of the porphyrins are predominantly determined by the four frontier orbitals, HOMO-1, HOMO, LUMO, and LUMO+1 [62,63], which is often referred to as the Gouterman 4-orbital model. The rotational freedom of the phenyl rings breaks the porphin molecular orbital symmetry and allows mixing [64]. Consequently, the LUMO and LUMO+1 assume a slightly different form compared to H2P (porphin). We have seen that the Gouterman orbitals of H2TPP remain practically identical to vacuum counterparts at the surface, even when interacting with the step edge or the kink site (cf. Fig. 4). Once metalated, the interaction of MgTPP with the kink site and the step edge is more substantial, and the resulting Gouterman-like orbitals spread over a more expansive energy window, intermixing with MgO Oxygen states (cf. Figs. 5 and 6).

The O_{3C} at kink site and the nearby O_{4c} are both known to be charged color centers [65,66]. Before metalation, the iminic nitrogen is attracted to the O_{4C}, and after metalation Mg center stays directly on O_{3C}. The HOMO-1 of MgTPP extends slightly to O_{4C} directly below the nitrogen. The phenyl rings are known to act as electron donors. After metalation, we have observed a strongly localized virtual state between the phenyl ring and the O_{4c}.

In Figs. 7 and 8, we compare the level alignment resulting from PBE-VdW and the higher-ranked HSE06 functionals. The HSE06 functional opens the band gap of MgO while the HOMO-LUMO gap of the porphyrin is less affected. Whereas the PBE-VdW functional puts the HOMO-1 of H2TPP aligned at the valance band edge of MgO, the HSE06 predicts all H2TPP Gouterman orbitals as mid-gap states. This difference is mainly due to the scissor shift of MgO band edges in HSE06, the energy

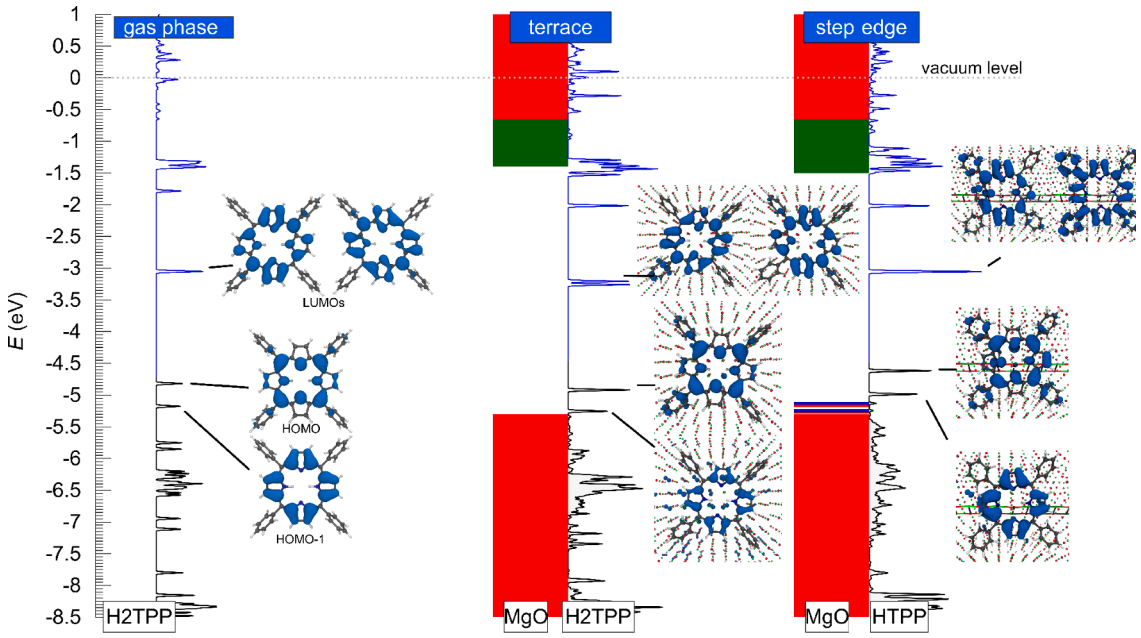

Fig. 4. Molecular orbitals of H2TPP and their energy alignment with the substrate states for H2TPP adsorbed at the terrace and the step edge using the PBE-VdW functional. Left: density of states of the H2TPP in the gas phase – the occupied states are indicated in black and unoccupied ones in blue; the electron density of the HOMO-1, HOMO, LUMO, and LUMO+1 that form the four Gouterman orbitals is shown as well. Middle: projected density of molecular orbitals of H2TPP adsorbed on the terrace alongside with the electron density of the four Gouterman orbitals; the MgO bulk and surface states are schematically indicated in orange and green. Right: same as in the middle panel for H2TPP adsorbed at the step edge; in addition, substrate states with strong localization at the step edge are indicated in blue. In all cases energy levels are aligned relative to the vacuum level indicated by the doted line. The four Gouterman orbitals do not interact with the substrate significantly, and appear within the energy gap of the substrate states.

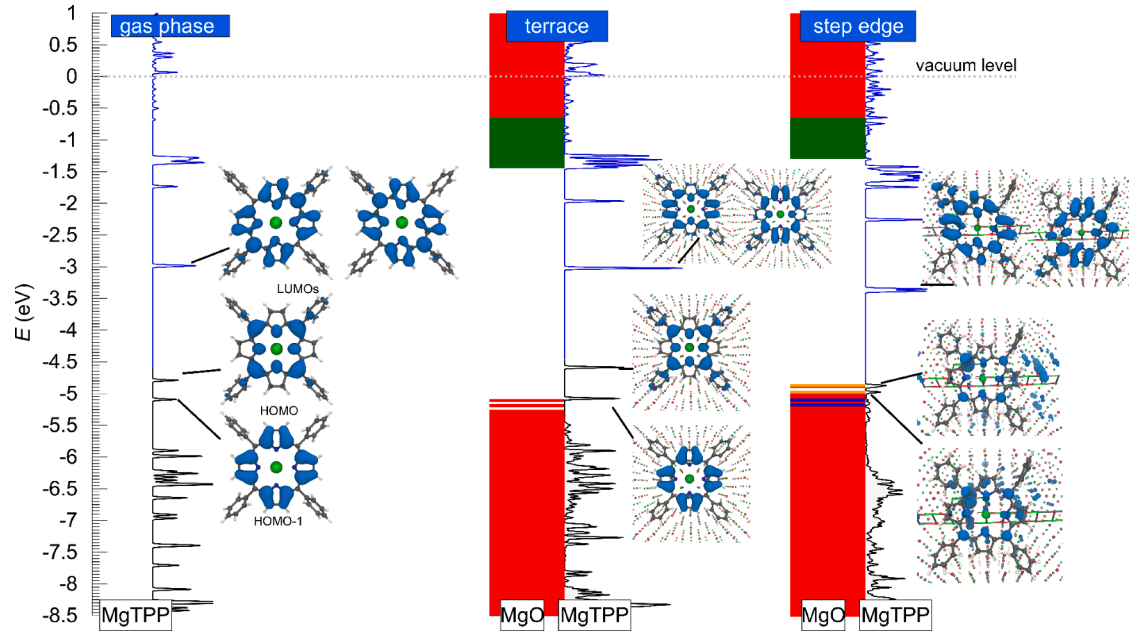

Fig. 5. Molecular orbitals of MgTPP and their energy alignment with the substrate states for MgTPP adsorbed at the terrace and after the metalation reaction at the step edge as obtained with the PBE-VdW functional. Left: density of states of the MgTPP in the gas phase; the electron density of the HOMO-1, HOMO, LUMO, and LUMO+1 that form the four Gouterman orbitals is shown as well. Middle: projected density of molecular orbitals of MgTPP adsorbed on the terrace alongside with the electron density of the four Gouterman orbitals; the position of MgO bulk and surface states are schematically indicated in orange and green. Right: same as in the middle panel for MgTPP after metalation at the step edge; substrate states with strong localization at the step edge as well as states of the hydroxylized Mg-vacancy interacting with MgTPP are indicated in blue and yellow respectively. In all cases energy levels are aligned relative to the vacuum level indicated by the doted line.

positions of H2TPP molecular orbitals do not shift as significantly. In PBE-VdW, all the Gouterman orbitals of H2TPP are essentially localized on the molecule. Thus, for all practical purposes, both HSE06 and PBE-VdW yield similar character for the frontier orbitals of the functionalized system. The only qualitative difference for MgTPP is the interaction with the hydroxylated Mg-vacancy at the step edge. In the description by the PBE-VdW, HOMO and HOMO-1 orbitals react with oxygen-related defect levels, which is not the case for the HSE06 results. In fact, as

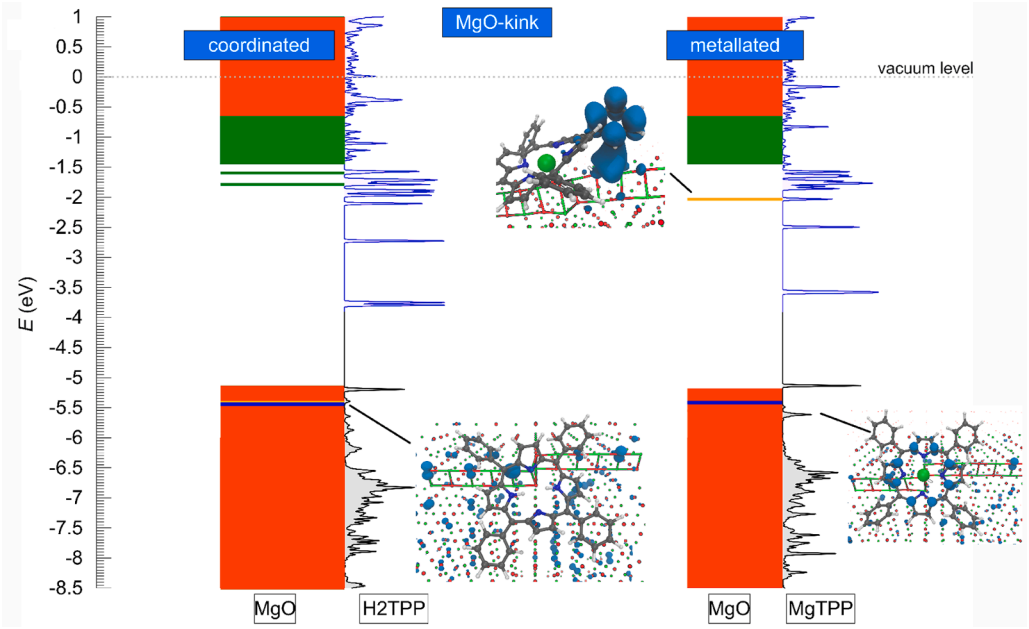

Fig. 6. Projected density of states of the porphyrin molecular orbitals and their alignment with substrate levels at the Mg-kink site before and after metalation. Left: H2TPP coordinated with the Mg-kink site before the dehydroxilation and subsequent metalation reaction. Right: MgTPP at the kink-site after metalation; the Mg-kink is converted into a hydroxylated O-kink. In both panels, the position of MgO bulk, surface, and step edge related states are schematically indicated in orange, green, and blue respectively. Note that the porphyrin strongly interacts with the kink site. For the corresponding states, the substrate part is schematically indicated in yellow and their electron density is shown. The most notable features are a low-lying charge transfer state to step-edge oxygen, and after metalation, a high lying charge trap that lies between the phenyl ring and the O_{4c}.

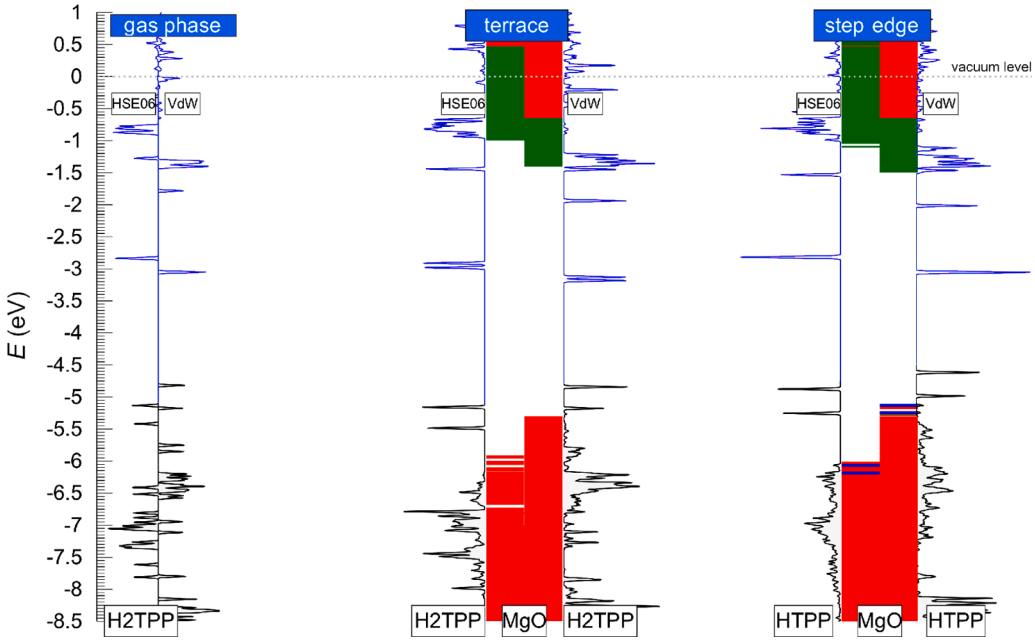

Fig. 7. Comparison of the level alignment obtained using the PBE-VdW and HSE06 functionals for H2TPP in the gas phase (left), at the terrace (middle), and at the step edge (right). In all panels the projected density of states of H2TPP is shown alongside a schematic representation of the position substrate states; bulk states are indicated in orange and surface states in green (see also Figs. 4 and 5). Energy levels are aligned to the vacuum level as a common reference. The comparison is based on the same snapshots in both cases.

shown in Fig. 8, the defect state (in yellow) are placed closer to the valance band edge and alignment with HOMO, HOMO-1, whereas the HSE06 shifts them to lower energies, away from the molecular states.

In Fig. 9, we illustrate how the *GW* level of theory would affect the level alignment. We have shown that the vacuum level provides for these systems a robust reference point for comparing calculations with different functionals or the separated porphyrin and substrate [42,44,61]. Here, we perform separate *GW* calculations on isolated H2TPP and MgO surface as the treatment of the adsorbed H2TPP is computationally to expensive. Alongside with an alignment to the common vacuum level, the results already give relevant insight into the level alignment of the adsorbed porphyrin [44,61]. We compare this level scheme with a PBE-VdW calculation of H2TPP on the MgO(001) terrace. The findings for the valence, surface, and conduction band edges of the MgO(100) surface within *GW* nicely agree with corresponding experimental values [67]. The *GW* opens the HOMO-LUMO gap of the H2TPP molecule much more than the HSE06 calculation, by pushing the unoccupied LUMO up. The H2TPP LUMO obtained from the *GW* calculation is positioned closer to the unoccupied surface band as compared both to the HSE06 and PBE-VdW results, which are found rather at mid gap. We would like to emphasize that, since the *GW* calculation is performed on the isolated H2TPP, the result lacks renormalization due to the adsorption at surface, such as image potential effects. This renormalization would naturally be included in fully-fledged, yet numerically too expensive GW calculation of the adsorbate system. For benzene at MgO(001), the simplest aromatic adsorbate [68] the level shift amounts to 0.5 eV [68]. Level shifts of a porphyrin adsorbed at the terrace, step edge, or Mg-kink were estimated [44] to 0.53 eV, 0.86 eV, or 0.76 eV, respectively.

To sum up, we report that the energy position and appearance of Gouterman molecular levels are very similar in the adsorbed state and

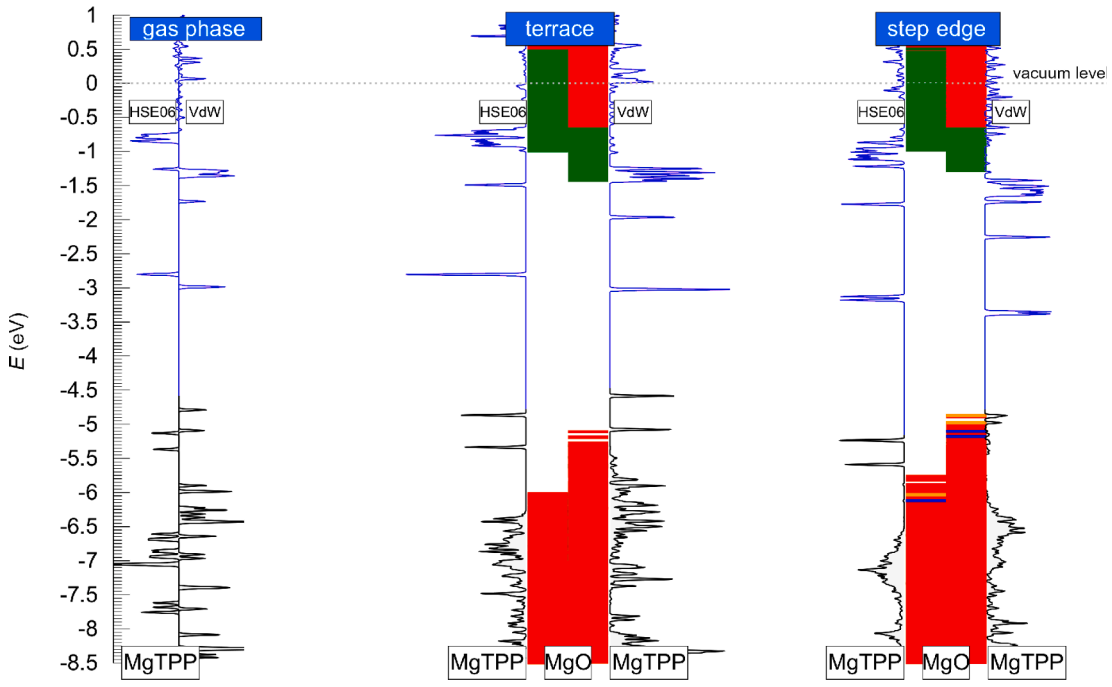

Fig. 8. Comparison of the level alignment obtained using the PBE-VdW and HSE06 functionals for MgTPP in the gas phase (left), at the terrace (middle), and at the step edge (right). In all panels the projected density of states of MgTPP is shown alongside a schematic representation of the substrate states; bulk states are indicated in orange and surface states in green (see also Figs. 4 and 5). The comparison is based on the same snapshot in both cases.

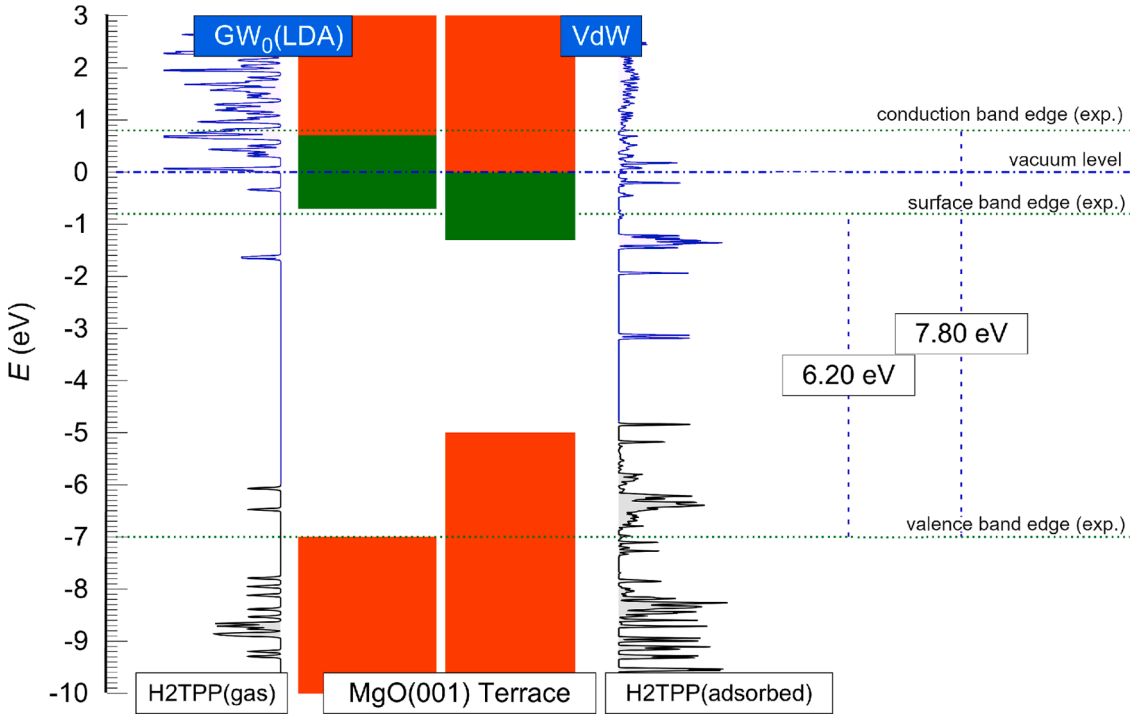

Fig. 9. Comparison of the level alignment obtained from the PBE + VdW, GW_0/G_0W_0 for H2TPP in the gas phase and the MgO(100) terrace. Left and right most panels: projected density of states of H2TPP in the gas phase and adsorbed at the terrace (GW_0 and PBE-VdW, repesctively). Middle panels: schematic representation of the MgO bulk and surface level positions (G_0W_0 and PBE-VdW) indicated in orange and green, respectively; the type of calculation is as noted. Energy levels are aligned to the vacuum level as a common energy reference. Experimental findings taken from Ref. [67] are indicated as well.

the gas phase in both HS06 and PBE-VdW. The notable exception is the complex of MgTPP with the hydroxylated Mg step-edge vacancy, for which the PBE-VdW predicts an intermixing of MgTPP HOMO-1 and HOMO with substrate states, whereas HSE06 does not. Both HSE06 and PBE-VdW lack long-range correlation effects, among which image potential effects are the most important. The quasiparticle energies of the *GW* would include such renormalization on the order 0.5–0.9 eV [44, 68]. However, the renormalization would not alter our conclusions and is beyond the scope of the present work, as it would require unaffordable numerical effort.

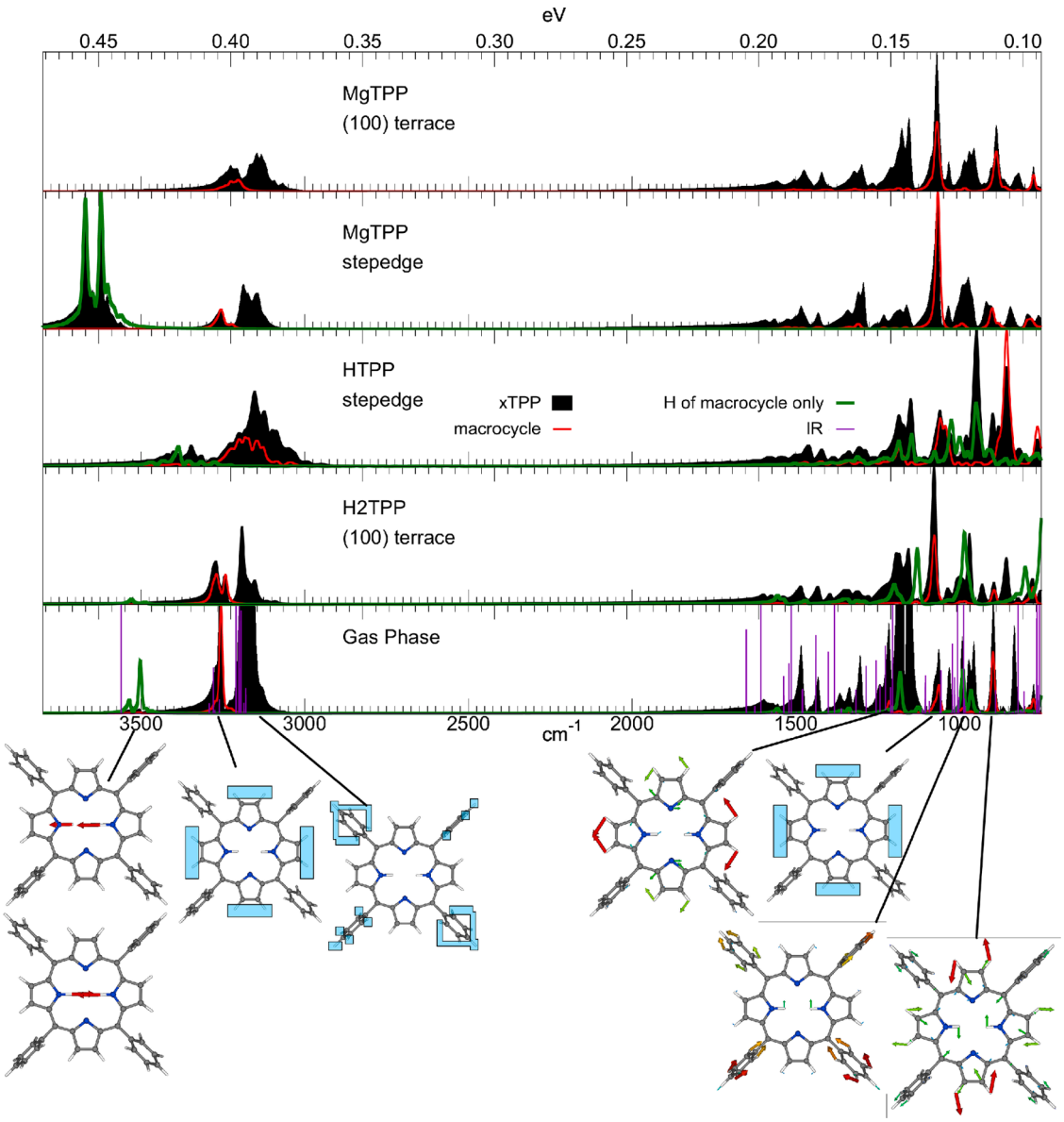

Fig. 10. Density of vibrational modes of H2TPP and MgTPP at various configurations. Panels from the lower panel to the top: H2TTP at gas phase, H2TPP adsorbed on the terrace, H2TPP deprotonated (HTPP), MgTPP at step edge, and MgTPP adsorbed on the terrace. The vibrational modes that involve macrocycle atoms are indicated in red. Vibrational modes involving Hydrogen initially bound to aminic nitrogen are indicated in green. The intensities of the red and green outlines were scaled for better visibility. For comparison, the IR absorption spectrum calculated using perturbation theory together with the HSE06 functional is indicated in purple.

3.3. Vibrational fingerprints of the metalation

The molecular dynamics simulation gives access to vibrational spectra through the velocity autocorrelation function. Furthermore, the velocity autocorrelation function allows selecting a subset of atoms and calculating their contribution to vibrational spectra. This is especially useful in the case of porphyrins, where a mode-by-mode analysis is unyielding due to the flexibility of the macrocycle leading to a band of close-lying vibrational modes. We report that the Hydrogen initially bound to aminic nitrogen can be used to trace the current state of the porphyrin. When H2TPP deprotonates at the step edge, this hydrogen mode redshifts. Once the metalation has occurred, the surface hydroxyl groups oscillate at a much higher rate, distinct from any macrocycle –N–H vibration. The MgO vibrational levels lie at a much higher frequency and do not interfere with the picture.

The fast vibronic excited states of porphyrins are known to strongly influence the level alignments and the spectral footprint, resulting in effects such as dynamical charge transfer states [64,69,70]. Although vibronic coupling is beyond the scope of this work, a brief look how the vibronic features shift will provide valuable insight on how the functionalization affects the porphyrin

Three energy ranges can be used for characterizing the continuum of porphyrin modes. The highest energy modes are due to Hydrogen attached to aminic nitrogen (around 3500 cm^{-1}). The second range of 3000–3250 cm^{-1} contains two prominent peaks, one due to porphin hydrogen modes and one due to phenyl ring hydrogen modes. The lower energy range extends from 1600 cm^{-1} onwards. When the porphyrin interacts with the surface, the high-energy windows virtually remain the same. However, the collection of porphin in-plane modes at around 1209 cm^{-1} and 884 cm^{-1} get clamped. The relative intensity of Hydrogen bending and stretching modes at around 1054 cm^{-1} with respect to these other two mode collections is enhanced. The rise of 884 cm^{-1} mode when deprotonation occurs is significant since at this energy

window in the H2TPP gas phase, the Hydrogen attached to aminic nitrogen vibrate in a bending mode that would allow the phototautomerization effect, and this might be the driving force where the second Hydrogen of HTPP will tautomerize and allow the exchange reaction. Another prominent sign of deprotonation is the redshift of high-energy aminic hydrogen stretching mode. After metalation, the Hydrogen previously attached to aminic nitrogen forms hydroxyl groups on the surface. The associated vibrational stretching modes are blue-shifted with respect to the previous stretching modes (~ 3600 cm^{-1}). Furthermore, the contribution of porphin to ~ 1209 cm^{-1} modes become negligible (predictably, since Mg is now interacting with N), and the Hydrogen bending and stretching modes at ~ 1054 cm^{-1} again becomes the predominant macrocycle feature at the lower energy window. The out-of-plane macrocycle modes have much lower energy, around 112 cm^{-1}, and will not be discussed in this context.

4. Conclusion

In this work, we performed and analyzed ab initio molecular dynamics simulation of the interaction of H2TPP and MgTPP with MgO (001) surface, the (100)-oriented step edge, and an Mg-kink. The porphyrins remain uncharged when adsorbed at the surface, corresponding in experiments to the bulk terminated MgO, MgO nanocubes, and thick MgO films on metal substrates. Both porphyrins are found to be mobile on MgO(001) terrace. Their motion is driven by a tug-of-war between the preference of the phenyl rings to be aligned at an angle with the macrocycle and a strong attraction of the flexible macrocycle to the surface. Our main focus is on the interaction of the free-base porphyrin with low-coordinated sites. Fast deprotonation and subsequent energy-driven metalation occur at common step edge and less common kink sites. The metalation at low-coordinated surface sites and migration back to surface (or even desorption) is energy driven (see Fig. 1). Metalated MgTPP is less bound to the reaction site due to the dynamics of phenyl rings. Overall, the dynamic effect renormalizes the reaction energies by about 1 eV. The state of the porphyrin metalation can be observed through aminic nitrogen vibrational levels. The physisorption leaves the Gouterman symmetry cascade argument applicable when the molecule is on the pristine terrace and before metalation at extended defects.

Credit author statement

O. B. M. and M. B. conceived the work. M. B. was responsible for the Methodology, while O. B. M. performed the investigation including the formal analysis visualization under supervision of M. B.. Both authors jointly wrote, reviewed, and edited the original draft.

Declaration of Competing Interest

The authors declare that they have no known competing financial interests or personal relationships that could have appeared to influence the work reported in this paper.

Acknowledgments

The authors acknowledge valuable discussions with Th. Fauster, Peter Puschnig, and Martin Sterrer. This project is part of the DFG Research Unit FOR 1878, and has been funded by Deutsche Forschungsgemeinschaft (grant: BO 1851/4-1) and Austrian FWF (grant: I 3385-N34). Computer time was provided on the HPC cluster at the RRZE of Friedrich-Alexander University Erlangen-Nürnberg and on the Doppler-Cluster of the Paris-Lodron University Salzburg.

References

[1] J.M. Gottfried, Surface chemistry of porphyrins and phthalocyanines, Surf. Sci. Rep. 80 (3) (2015) 259–379, https://doi.org/10.1016/j.surfrep.2015.04.001, http://www.sciencedirect.com/science/article/pii/S0167572915000114.

[2] M. Borgström, E. Blart, G. Boschloo, E. Mukhtar, A. Hagfeldt, L. Hammarström, F. Odobel, Sensitized hole injection of phosphorus porphyrin into NiO: toward new photovoltaic devices, J. Phys. Chem. B 109 (48) (2005) 22928–22934, https://doi.org/10.1021/jp054034a. PMID: 16853987, https://doi.org/10.1021/jp054034a.

[3] W. Auwärter, K. Seufert, F. Bischoff, D. Ecija, S. Vijayaraghavan, S. Joshi, F. Klappenberger, N. Samudrala, J.V. Barth, A surface-anchored molecular four-level conductance switch based on single proton transfer, Nat. Nanotechnol. 7 (1) (2012) 41.

[4] Y. Sivalingam, E. Martinelli, A. Catini, G. Magna, G. Pomarico, F. Basoli, R. Paolesse, C. Di Natale, Gas-sensitive photoconductivity of porphyrin-functionalized ZnO nanorods, J. Phys. Chem. C 116 (16) (2012) 9151–9157, https://doi.org/10.1021/jp302225u.

[5] T. Hasobe, Porphyrin-based supramolecular nanoarchitectures for solar energy conversion, J. Phys. Chem. Lett. 4 (11) (2013) 1771–1780, https://doi.org/10.1021/jz4005152. PMID: 26283108, https://doi.org/10.1021/jz4005152.

[6] M. Urbani, M. Gratzel, M.K. Nazeeruddin, T. Torres, Meso-substituted porphyrins for dye-sensitized solar cells, Chem. Rev. 114 (2014) 12330–12396.

[7] A. Maufroy, L. Favereau, F.B. Anne, Y. Pellegrin, E. Blart, M. Hissler, D. Jacquemin, F. Odobel, Synthesis and properties of push–pull porphyrins as sensitizers for NiO based dye-sensitized solar cells, J. Mater. Chem. A 3 (2015) 3908–3917, https://doi.org/10.1039/C4TA05974C.

[8] R. Paolesse, S. Nardis, D. Monti, M. Stefanelli, C. Di Natale, Porphyrinoids for chemical sensor applications, Chem. Rev. 117 (4) (2017) 2517–2583, https://doi.org/10.1021/acs.chemrev.6b00361. PMID: 28222604, https://doi.org/10.1021/acs.chemrev.6b00361.

[9] H. Song, Q. Liu, Y. Xie, Porphyrin-sensitized solar cells: systematic molecular optimization, coadsorption and cosensitization, Chem. Commun. 54 (2018) 1811–1824, https://doi.org/10.1039/C7CC09671B, https://doi.org/10.1039/C7CC09671B.

[10] T. Lukasczyk, K. Flechtner, L.R. Merte, N. Jux, F. Maier, J.M. Gottfried, H.-P. Steinrück, Interaction of cobalt(II) tetraarylporphyrins with a Ag(111) surface studied with photoelectron spectroscopy, J. Phys. Chem. C 111 (7) (2007) 3090–3098, https://doi.org/10.1021/jp0652345.

[11] J. Schneider, M. Franke, M. Gurrath, M. Rockert, T. Berger, J. Bernardi, B. Meyer, H.P. Steinruck, O. Lytken, O. Diwald, Porphyrin metalation at MgO surfaces: a spectroscopic and quantum mechanical study on complementary model systems, Chemistry 22 (5) (2016) 1744–1749.

[12] C.C. Fernndez, D. Wechsler, T.C. Rocha, H.-P. Steinrück, O. Lytken, F.J. Williams, Adsorption geometry of carboxylic acid functionalized porphyrin molecules on TiO_2(110), Surf. Sci. 689 (2019) 121462, https://doi.org/10.1016/j.susc.2019.121462. http://www.sciencedirect.com/science/article/pii/S0039602819302778.

[13] G. Zamborlini, D. Lüftner, Z. Feng, B. Kollmann, P. Puschnig, C. Dri, M. Panighel, G. Di Santo, A. Goldoni, G. Comelli, et al., Multi-orbital charge transfer at highly oriented organic/metal interfaces, Nat. Commun. 8 (1) (2017) 335.

[14] J.V. Barth, G. Costantini, K. Kern, Engineering atomic and molecular nanostructures at surfaces, Nature 437 (7059) (2005) 671–679.

[15] F.S. Kim, G. Ren, S.A. Jenekhe, One-dimensional nanostructures ofπ-conjugated molecular systems: assembly, properties, and applications from photovoltaics, sensors, and nanophotonics to nanoelectronics, Chem. Mat. 23 (3) (2011) 682–732.

[16] G.C. La Rocca, Organic photonics polariton lasing, Nat. Photonics 4 (6) (2010) 343–345.

[17] D.M. Coles, N. Somaschi, P. Michetti, C. Clark, P.G. Lagoudakis, P.G. Savvidis, D. G. Lidzey, Polariton-mediated energy transfer between organic dyes in a strongly coupled optical microcavity, Nat. Mater. 13 (7) (2014) 712–719.

[18] H. Marbach, Surface-mediated in situ metalation of porphyrins at the solid-vacuum interface, Acc. Chem. Res. 48 (9) (2015) 2649–2658, https://doi.org/10.1021/acs.accounts.5b00243. PMID: 26308682, https://doi.org/10.1021/acs.accounts.5b00243.

[19] K. Diller, A.C. Papageorgiou, F. Klappenberger, F. Allegretti, J.V. Barth, W. Auwärter, In vacuo interfacial tetrapyrrole metallation, Chem. Soc. Rev. 45 (2016) 1629–1656, https://doi.org/10.1039/C5CS00207A, https://doi.org/10.1039/C5CS00207A.

[20] C. Wang, Q. Fan, Y. Han, J.I. Martinez, J.A. Martin-Gago, W. Wang, H. Ju, J. M. Gottfried, J. Zhu, Metalation of tetraphenylporphyrin with nickel on a TiO_2 (110)-1 $\times$ 2 surface, Nanoscale 8 (2) (2016) 1123–1132.

[21] Z. Wang, Z. Li, C.J. Medforth, J.A. Shelnutt, Self-assembly and self-metallization of porphyrin nanosheets, J. Am. Chem. Soc. 129 (9) (2007) 2440–2441.

[22] W. Auwarter, A. Weber-Bargioni, S. Brink, A. Riemann, A. Schiffrin, M. Ruben, J. V. Barth, Controlled metalation of self-assembled porphyrin nanoarrays in two dimensions, Chemphyschem 8 (2) (2007) 250–254.

[23] C. Wang, Q. Fan, S. Hu, H. Ju, X. Feng, Y. Han, H. Pan, J. Zhu, J.M. Gottfried, Coordination reaction between tetraphenylporphyrin and nickel on a TiO_2(110) surface, Chem. Commun. (Camb) 50 (61) (2014) 8291–8294.

[24] G. Lovat, D. Forrer, M. Abadia, M. Dominguez, M. Casarin, C. Rogero, A. Vittadini, L. Floreano, Hydrogen capture by porphyrins at the TiO_2(110) surface, Phys. Chem. Chem. Phys. 17 (44) (2015) 30119–30124.

[25] J. Köbl, T. Wang, C. Wang, M. Drost, F. Tu, Q. Xu, H. Ju, D. Wechsler, M. Franke, H. Pan, H. Marbach, H.-P. Steinrück, J. Zhu, O. Lytken, Hungry porphyrins: protonation and self-metalation of tetraphenylporphyrin on TiO_2(110) - 1 $\times$ 1, ChemistrySelect 1 (2016) 6103–6105.

[26] G. Lovat, D. Forrer, M. Abadia, M. Dominguez, M. Casarin, C. Rogero, A. Vittadini, L. Floreano, On-surface synthesis of a pure and long-range-ordered titanium(IV)-porphyrin contact layer on titanium dioxide, J Phys. Chem. 121 (2017) 13738–13746.

[27] J. Schneider, F. Kollhoff, J. Bernardi, A. Kaftan, J. Libuda, T. Berge, M. Laurin, O. Diwald, Porphyrin metalation at the MgO nanocube/toluene interface, ACS Appl. Mater. Interfaces 7 (2015) 22962–22969.

[28] G. Di Filippo, A. Classen, R. Poschel, T. Fauster, Interaction of free-base tetraphenylporphyrin with magnesium oxide: influence of MgO morphology on metalation, J. Chem. Phys. 146 (6) (2017) 064702.

[29] L. Egger, M. Hollerer, C.S. Kern, H. Herrmann, P. Hurdax, A. Haags, X. Yang, A. Gottwald, M. Richter, S. Soubatch, F.S. Tautz, G. Koller, P. Puschnig, M. G. Ramsey, M. Sterrer, Charge-promoted self-metalation of porphyrins on an oxide surface, Angew. Chem. Int. Ed. 60 (2021) 5078–5082.

[30] D. Wechsler, C.C. Fernandez, Q. Tariq, N. Tsud, K.C. Prince, F. J.Williams, H.-P. Steinrück, O. Lytken, Interfacial reactions of tetraphenylporphyrin with cobalt-oxide thin films, Chem. Eur. J. 25 (2019) 13197–13201.

[31] C. Wang, R. Wang, J. Hauns, T. Fauster, Self-metalation of porphyrins by cobalt oxide: photoemission spectroscopic investigation, J. Phys. Chem. C 124 (2020) 14167–14175.

[32] A. Calloni, M. Jagadeesh, G. Bussetti, G. Fratesi, S. Achilli, A. Picone, A. Lodesani, A. Brambilla, C. Goletti, F. Ciccacci, L. Duș, M. Finazzi, A. Goldoni, A. Verdini, L. Floreano, Cobalt atoms drive the anchoring of Co-TPP molecules to the oxygen-passivated Fe(001) surface, Appl. Surf. Sci. 505 (2020) 144213, https://doi.org/10.1016/j.apsusc.2019.144213, http://www.sciencedirect.com/science/article/pii/S0169433219330296.

[33] G. Fratesi, S. Achilli, A. Ugolotti, A. Lodesani, A. Picone, A. Brambilla, L. Floreano, A. Calloni, G. Bussetti, Nontrivial central-atom dependence in the adsorption of M-TPP molecules (M = Co, Ni, Zn) on Fe(001)-p(1 × 1)O, Appl. Surf. Sci. 530 (2020) 147085, https://doi.org/10.1016/j.apsusc.2020.147085. http://www.sciencedirect.com/science/article/pii/S0169433220318420.

[34] P.V. Sushko, A.L. Shluger, Electronic structure of excited states at low-coordinated surface sites of MgO, Surf. Sci. 421 (3) (1999) L157–L165.

[35] G. Kresse, J. Furthmüller, Software VASP, Vienna (1999), Phys. Rev. B 54 (11) (1996) 169.

[36] P. Hohenberg, W. Kohn, Inhomogeneous electron gas, Phys. Rev. 136 (3B) (1964) B864–B871.

[37] W. Kohn, L.J. Sham, Self-consistent equations including exchange and correlation effects, Phys. Rev. 140 (4A) (1965) A1133–A1138.

[38] S. Grimme, J. Antony, S. Ehrlich, H. Krieg, A consistent and accurate ab initio parametrization of density functional dispersion correction (DFT-D) for the 94 elements H-Pu, J. Chem. Phys. 132 (15) (2010) 154104.

[39] T. Bucko, S. Lebegue, J.G. Angyan, J. Hafner, Extending the applicability of the Tkatchenko–Scheffler dispersion correction via iterative Hirshfeld partitioning, J. Chem. Phys. 141 (2014) 034114.

[40] A. Tkatchenko, R.A. DiStasio, R. Car, M. Scheffler, Accurate and efficient method for many-body van der Waals interactions, Phys. Rev. Lett. 108 (2012) 236402.

[41] J.P. Perdew, K. Burke, M. Ernzerhof, Generalized gradient approximation made simple, Phys. Rev. Lett. 77 (1996) 3865–3868, https://doi.org/10.1103/PhysRevLett.77.3865, https://link.aps.org/doi/10.1103/PhysRevLett.77.3865.

[42] O.B. Malcıoğlu, I. Bechis, M. Bockstedte, Effect of crystallization on the electronic and optical properties of archetypical porphyrins, Phys. Chem. Chem. Phys. 22 (2020) 3825.

[43] J.P. Perdew, A. Zunger, Selfinteraction correction to density-functional approximations for many electron systems, Phys. Rev. B 23 (1981) 5048.

[44] S. Ninova, O.B. Malcıoğlu, P. Auburger, M. Franke, O. Lytken, H.-P. Steinrück, M. Bockstedte, Morphology dependent interaction between Co(II)-tetraphenylporphyrin and the MgO(100) surface, Phys. Chem. Chem. Phys. 23 (2021) 2105.

[45] A.V. Krukau, O.A. Vydrov, A.F. Izmaylov, G.E. Scuseria, Influence of the exchange screening parameter on the performance of screened hybrid functionals, J. Chem. Phys. 125 (22) (2006) 224106, https://doi.org/10.1063/1.2404663, https://doi.org/10.1063/1.2404663.

[46] P. Pulay, Convergence acceleration of iterative sequences. the case of SCF iteration, Chem. Phys. Lett. 73 (2) (1980) 393–398.

[47] D.M. Wood, A. Zunger, A new method for diagonalising large matrices, J. Phys. A. 18 (9) (1985) 1343–1359.

[48] R.P. Feynman, Forces in molecules, Phys. Rev. 56 (4) (1939) 340–343.

[49] D. Levesque, L. Verlet, Molecular dynamics and time reversibility, J. Stat. Phys. 72 (3–4) (1993) 519–537.

[50] W.G. Hoover, Canonical dynamics: equilibrium phase-space distributions, Phys. Rev. A 31 (3) (1985) 1695–1697.

[51] S. Nosé, A molecular dynamics method for simulations in the canonical ensemble, Mol. Phys. 52 (2) (2006) 255–268.

[52] J.B. Bates, M.H. Brooker, Determination of longitudinal optical mode frequencies by polarized specular reflectance infrared spectroscopy, J. Phys. Chem. Solids 32 (10) (1971) 2403–2407.

[53] J.R. Jasperse, A. Kahan, J.N. Plendl, S.S. Mitra, Temperature dependence of infrared dispersion in ionic crystals LiF and MgO, Phys. Rev. 146 (2) (1966) 526–542.

[54] M.J.L. Sangster, G. Peckham, D.H. Saunderson, Lattice dynamics of magnesium oxide, J. Phys. C 3 (5) (1970) 1026–1036.

[55] O. Schütt, P. Pavone, W. Windl, K. Karch, D. Strauch, Ab initiolattice dynamics and charge fluctuations in alkaline-earth oxides, Phys. Rev. B 50 (8) (1994) 3746–3753.

[56] L.J. Boucher, J.J. Katz, The infared spectra of metalloporphyrins (4000-160 cm-1), J. Am. Chem. Soc. 89 (6) (1967) 1340–1345.

[57] P. Bour, K. Zaruba, M. Urbanova, V. Setnicka, P. Matejka, Z. Fiedler, V. Kral, K. Volka, Vibrational circular dichroism of tetraphenylporphyrin in peptide complexes? A computational study, Chirality 12 (4) (2000) 191–198.

[58] E. Apr, E.J. Bylaska, W.A. de Jong, N. Govind, K. Kowalski, T.P. Straatsma, M. Valiev, H.J.J. van Dam, Y. Alexeev, J. Anchell, V. Anisimov, F.W. Aquino, R. Atta-Fynn, J. Autschbach, N.P. Bauman, J.C. Becca, D.E. Bernholdt, K. Bhaskaran-Nair, S. Bogatko, P. Borowski, J. Boschen, J. Brabec, A. Bruner, E. Cauŀt, Y. Chen, G.N. Chuev, C.J. Cramer, J. Daily, M.J.O. Deegan, T.H. Dunning, M. Dupuis, K.G. Dyall, G.I. Fann, S.A. Fischer, A. Fonari, H. Frȍchtl, L. Gagliardi, J. Garza, N. Gawande, S. Ghosh, K. Glaesemann, A.W. Gȍtz, J. Hammond, V. Helms, E.D. Hermes, K. Hirao, S. Hirata, M. Jacquelin, L. Jensen, B.G. Johnson, H. Jnsson, R.A. Kendall, M. Klemm, R. Kobayashi, V. Konkov, S. Krishnamoorthy, M. Krishnan, Z. Lin, R.D. Lins, R.J. Littlefield, A.J. Logsdail, K. Lopata, W. Ma, A. V. Marenich, J. Martin del Campo, D. Mejia-Rodriguez, J.E. Moore, J.M. Mullin, T. Nakajima, D.R. Nascimento, J.A. Nichols, P.J. Nichols, J. Nieplocha, A. Otero-de-la Roza, B. Palmer, A. Panyala, T. Pirojsirikul, B. Peng, R. Peverati, J. Pittner, L. Pollack, R.M. Richard, P. Sadayappan, G.C. Schatz, W.A. Shelton, D. W. Silverstein, D.M.A. Smith, T.A. Soares, D. Song, M. Swart, H.L. Taylor, G. S. Thomas, V. Tipparaju, D.G. Truhlar, K. Tsemekhman, T. Van Voorhis, Á. Vázquez-Mayagoitia, P. Verma, O. Villa, A. Vishnu, K.D. Vogiatzis, D. Wang, J. H. Weare, M.J. Williamson, T.L. Windus, K. Woliski, A.T. Wong, Q. Wu, C. Yang, Q. Yu, M. Zacharias, Z. Zhang, Y. Zhao, R.J. Harrison, Nwchem: past, present, and future, J. Chem. Phys. 152 (18) (2020) 184102, https://doi.org/10.1063/5.0004997, https://doi.org/10.1063/5.0004997.

[59] T.H. Dunning, Gaussian basis sets for use in correlated molecular calculations. I. The atoms boron through neon and hydrogen, J. Chem. Phys. 90 (2) (1989) 1007–1023, https://doi.org/10.1063/1.456153, https://doi.org/10.1063/1.456153.

[60] H. Onishi, C. Egawa, T. Aruga, Y. Iwasawa, Adsorption of Na atoms and oxygen-containing molecules on MgO(100) and (111) surfaces, Surf. Sci. 191 (1987) 479–491.

[61] A. Classen, R. Poschel, G. Di Filippo, T. Fauster, O.B. Malcıoğlu, M. Bockstedte, Electronic structure of tetraphenylporphyrin layers on Ag(100), Phys. Rev. B 95 (11) (2017) 115414.

[62] M. Gouterman, Spectra of porphyrins, J. Mol. Spectrosc. 6 (1961) 138–163.

[63] P.G. Seybold, M. Gouterman, Porphyrins, J. Mol. Spectrosc. 31 (1969) 1–13.

[64] M. Kruk, A. Karotki, M. Drobizhev, V. Kuzmitsky, V. Gael, A. Rebane, Two-photon absorption of tetraphenylporphin free base, J. Lumin. 105 (2003) 45–55.

[65] M. Sterrer, E. Fischbach, T. Risse, H.J. Freund, Geometric characterization of a singly charged oxygen vacancy on a single-crystalline MgO(001) film by electron paramagnetic resonance spectroscopy, Phys. Rev. Lett. 94 (2005) 186101.

[66] M. Sterrer, M. Heyde, M. Novicki, N. Nilius, T. Risse, H.P. Rust, G. Pacchioni, H. J. Freund, Identification of color centers on MgO(001) thin films with scanning tunneling microscopy, J. Phys. Chem. B 110 (2006) 46–49.

[67] S. Schintke, S. Messerli, M. Pivetta, F. Patthey, L. Libioulle, M. Stengel, A. De Vita, W.-D. Schneider, Insulator at the ultrathin limit: MgO on Ag(001), Phys. Rev. Lett. 87 (2001) 276801, https://doi.org/10.1103/PhysRevLett.87.276801, https://link.aps.org/doi/10.1103/PhysRevLett.87.276801.

[68] J.M. Garcia-Lastra, C. Rostgaard, A. Rubio, K.S. Thygesen, Polarization-induced renormalization of molecular levels at metallic and semiconducting surfaces, Phys. Rev. B 80 (2009) 245427, https://doi.org/10.1103/PhysRevB.80.245427.

[69] P.H. Kumar, Y. Venkatesh, D. Siva, B. Ramakrishna, P.R. Bangal, Ultrafast relaxation dynamics of 5,10,15,20-meso-Tetrakis pentafluorophenyl porphyrin studied by fluorescence up-conversion and transient absorption spectroscopy, J. Phys. Chem. A 119 (8) (2015) 1267–1278.

[70] S. Tognolini, S. Ponzoni, F. Sedona, M. Sambi, S. Pagliara, Role of the substrate orientation in the photoinduced electron dynamics at the porphyrin/Ag interface, J. Phys. Chem. Lett. 6 (2015) 3632–3638.